Tetrahedron 73 (2017) 4896–4900

Contents lists available at ScienceDirect

Tetrahedron

journal homepage: www.elsevier.com/locate/tet

A trypsin-based bistable switch☆

Sjoerd G.J. Postma, Dana te Brinke, Ilia N. Vialshin, Albert S.Y. Wong, Wilhelm T.S. Huck*

Radboud University, Institute for Molecules and Materials, Heyendaalseweg 135, 6525 AJ, Nijmegen, The Netherlands

ARTICLE INFO

Article history:
Received 6 March 2017
Received in revised form
20 April 2017
Accepted 21 April 2017
Available online 26 April 2017

Keywords:
Complex behavior
Reaction networks
Bistability
Enzymes

ABSTRACT

Recreating some of the emergent behavior seen in biological reaction networks is an important goal in the new field of systems chemistry. One of the classic examples of complex behavior is bistability, which is abundantly used in living organisms for switching between cellular states. Here, we create a bistable switch based on the autocatalytic activation and inhibition of the enzyme trypsin under flow conditions. We investigate the influence of the inhibitor structure, and hence inhibition kinetics, on the properties of the bistable switch.

1. Introduction

All-or-none responses are crucial in cellular processes such as differentiation,[1] cell motility,[2] apoptosis,[3] and cell cycle control.[4,5] This type of response is typically regulated by bistable switches,[6–8] that are able to maintain a stable state A until a trigger switches the system to state B, after which this new state persists even when the trigger is removed, a property called hysteresis. In the past decades, artificial networks have been developed that display bistability, including ones based on DNA circuits,[9] enzymes,[10] inorganic chemistry,[11] and most recently, small organic molecules.[12] In addition, mathematical analyses have indicated that many network motifs can lead to bistability as long as they contain a sufficient degree of nonlinear kinetics.[13,14] We propose to use a basic motif, displayed in Fig. 1A, where an autocatalytic, positive feedback loop in which trypsin (Tr) catalyzes its own formation from its precursor trypsinogen (Tg), is combined with a trypsin inhibitor (Inh). Importantly, trypsinogen displays self-activation due to residual tryptic activity, which ensures a slow, but continuous production of trypsin.[15] This motif is comparable with the one that was described recently, in which thiols were constantly produced through thioester hydrolysis, amplified through native chemical ligation, and inhibited by maleimides.[12] Importantly, bistability is only obtained under out-of-equilibrium conditions in these systems, and to that end we implement a flow reactor.

In this report, we achieve bistability by combining kinetic studies with batch experiments and computational modelling to predict the conditions necessary for bistability in a flow reactor. Previously, we developed this strategy to design a trypsin oscillator based on a different network motif than the one used here.[16] Furthermore, we now synthesize a new, more potent inhibitor of trypsin by modifying a commercially available trypsin inhibitor, and probed the influence of the inhibition kinetics on the properties of the bistable system. As we saw before in the trypsin oscillator,[17] small modifications in molecular structure can have a profound influence on the behavior of complex, out-of-equilibrium networks.

2. Results and discussion

In a reactor, the autocatalytic formation of trypsin is antagonized by the outflow of reaction products.[18] Intuitively, at extremely high flow rates, the outflow of the reactor is similar to its inflow, because trypsinogen is washed out of the reactor before it can be activated. Conversely, one imagines that under batch conditions (no flow) the reaction will proceed until all trypsinogen has been converted into trypsin and thermodynamic equilibrium is reached. Under all circumstances, the addition of inhibitor counteracts the autocatalysis. In a bistable system, a regime exists in which the starting concentration of trypsin determines the final state of the system. At low concentrations of trypsin, outflow and inhibition

☆ The authors congratulate Prof Ben Feringa on being awarded the 2016 Tetrahedron Prize and Nobel Prize in Chemistry.

* Corresponding author.
E-mail address: w.huck@science.ru.nl (W.T.S. Huck).

http://dx.doi.org/10.1016/j.tet.2017.04.053

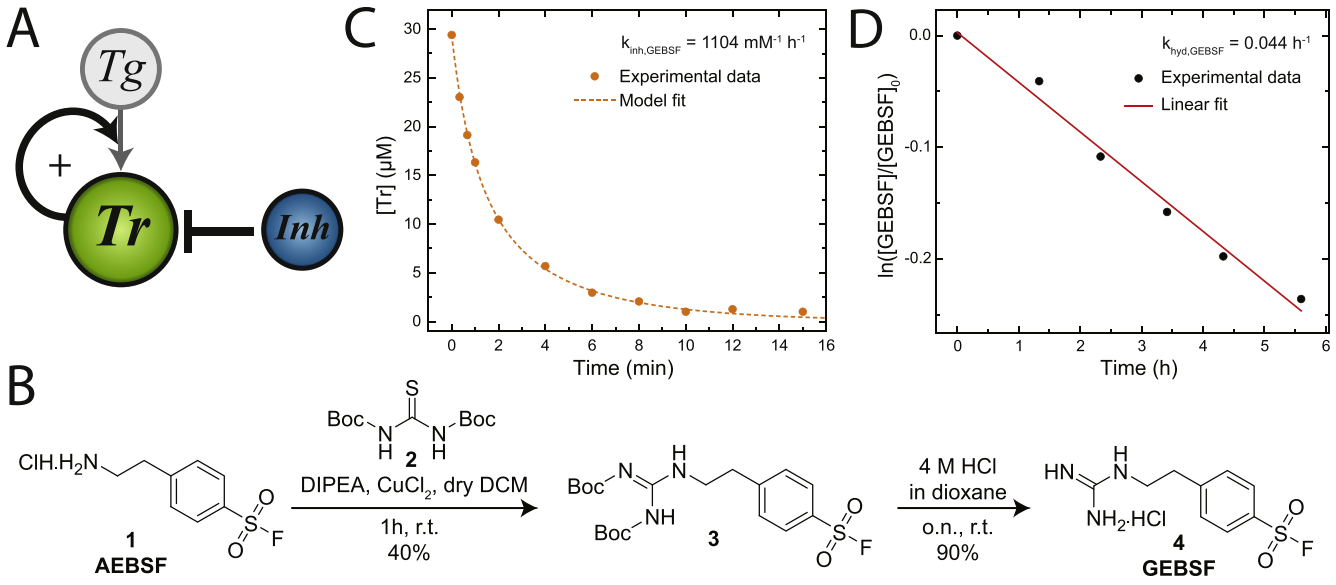

Fig. 1. A) The enzymatic reaction network used to obtain bistability. Trypsin is autocatalytically produced from trypsinogen, but deactivated by an inhibitor. **B)** Modification of the trypsin inhibitor AEBSF by guanylation of its amine. Details of the synthesis are in the Experimental Section. **C)** Inhibition of trypsin ($[Tr]_0$ = 29.4 μM) by GEBSF ($[GEBSF]_0$ = 40 μM) in 0.1 M Tris-HCl, pH 7.7, 20 mM $CaCl_2$ at 22 °C. The experimental data (dots) were fitted by a bimolecular reaction model in COPASI (dashed line). **D)** Hydrolysis of the sulfonyl fluoride of GEBSF as followed by ^{1}H NMR in 50 mM Tris-HCl, pD 7.7, in D_2O containing 20 mM $CaCl_2$ at 22 °C. The experimental data (dots) were fitted in Origin (solid line). Abbreviations: Tg = trypsinogen, Tr = trypsin, Inh = inhibitor, AEBSF = 4-(2-aminoethyl)benzenesulfonyl fluoride, GEBSF = 4-(2-guanidinoethyl)benzenesulfonyl fluoride.

outcompete autocatalysis, but at higher concentrations of trypsin, the rate of autocatalysis is increased tremendously due to its nonlinear nature, and a high concentration of trypsin is maintained.

Therefore, it is necessary for the inhibitor to strongly oppose trypsin formation (*i.e.* relatively high rate of inhibition), while allowing the trypsin concentration to quickly increase when autocatalysis outcompetes inhibition (for instance when all inhibitor has reacted). These are the properties we are looking for below, when we test two different trypsin inhibitors.

2.1. Synthesis and kinetic studies of potent inhibitor

First, we synthesized an arginine-like analogue of the commercially available trypsin inhibitor 4-(2-aminoethyl)benzenesulfonyl fluoride (AEBSF, compound **1** in Fig. 1b) by guanylating its amine using a standard two-step procedure (Fig. 1A).[19] In the first step, AEBSF reacts with *N,N'*-di-boc-thiourea (**2**) to form a boc-protected guanidinium group (compound **3**), after which a simple boc-deprotection step yields the desired compound 4-(2-guanidinoethyl)benzenesulfonyl fluoride (GEBSF, **4**).

Next, we investigated the inhibitory properties by mixing GEBSF (40 μM) with trypsin (29.4 μM). The activity of trypsin was measured over time by a fluorogenic assay (see the Experimental section). Fig. 1C shows that trypsin is fully inhibited after 15 min (orange dots), indicating that GEBSF is indeed a potent inhibitor of trypsin. The experimental data were fitted to a bimolecular reaction model in COPASI (Fig. 1C, orange dashed lines), and a parameter estimation procedure resulted in a rate constant $k_{inh,GEBSF}$ of 1104 mM^{-1} h^{-1}. This value is much higher than the trypsin inhibition rate constant for AEBSF (53 mM^{-1} h^{-1}) we measured before, but also considerably larger than the k_{cat}/K_M value (a measure of enzymatic efficiency) of trypsinogen conversion by trypsin (63 mM^{-1} h^{-1}).[16] Therefore, it is expected that GEBSF would be more suitable to antagonize autocatalytic trypsin production than AEBSF.

Hydrolysis of the sulfonyl fluoride moiety is a side reaction that needs to be measured as well, as it results in a sulfonic acid that inhibits trypsin only weakly and reversibly. To that end, GEBSF was dissolved in deuterated buffer, and changes in the benzene ring peaks due to hydrolysis were monitored by ^{1}H NMR at 22 °C. The reaction was considered to be pseudo-first order, and a linear fit through experimental data points expressed as ln([GEBSF]/[GEBSF]$_0$) yielded a hydrolysis rate constant $k_{hyd,GEBSF}$ of 0.044 h^{-1} ($t_{½}$ = 15.8 h, Fig. 1D). This value is comparable with the hydrolysis rate constant for AEBSF (0.034 h^{-1}),[16] and will be taken into account in all computational models mentioned below. The weak, reversible inhibition of trypsin by the hydrolyzed inhibitor is not considered in the models, as initial calculations showed no significant effect thereof on the behavior of the network.

2.2. Batch experiments and modelling

Next, we tested the properties of the inhibitors in batch experiments in which thermodynamic equilibrium is inevitably reached. Trypsinogen (100 μM) is fully converted into trypsin within two hours in the absence of inhibitor, and the S-shaped activation curve is characteristic for autocatalytic reactions (orange dots in Fig. 2). The activation of trypsinogen is severely delayed in the presence of AEBSF (50–100 μM), and the S-shaped curve is much more gradual than in the absence of inhibitor (top panel in Fig. 2). The experiment with 100 μM AEBSF still yields a final trypsin concentration of about 40 μM due to significant hydrolysis of the inhibitor at this timescale. In contrast, lower concentrations (5–9 μM) of GEBSF are required to obtain a similar delay in activation as with high concentrations of AEBSF, because of the higher inhibition rate constant of GEBSF. Consequently, higher final concentrations of trypsin are obtained when GEBSF is used (bottom panel in Fig. 2). Moreover, in case of GEBSF the steepness of the activation curves strongly resembles the one in the absence of inhibitor.

Then, we built a model describing these batch experiments in COPASI to gain more insight in the differences between the inhibitors. In the model, four reactions are considered: 1) autoactivation of trypsinogen, 2) activation of trypsinogen by trypsin, 3) inhibition of trypsin by an inhibitor, 4) hydrolysis of the inhibitor. A

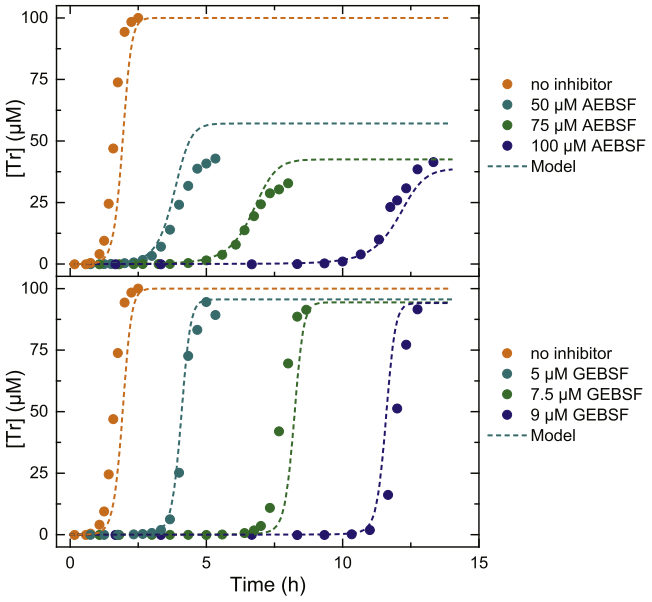

Fig. 2. Batch experiments in which trypsinogen ($[Tg]_0$ = 100 μM) was mixed with various concentrations of AEBSF (top panel) or GEBSF (bottom panel) 0.1 M Tris-HCl, pH 7.7, 20 mM $CaCl_2$ at 22 °C. The experimental data points (dots) were fitted with a genetic algorithm in COPASI (dashed lines).

genetic algorithm was employed to estimate the rate constant for autoactivation of trypsinogen, which resulted in a value of $2.3*10^{-3}$ mM^{-1} h^{-1}. Gratifyingly, the model fits (dashed lines in Fig. 2) were in excellent agreement with experimental data. Parameter estimation resulted in inhibition rate constants of 86 mM^{-1} h^{-1} for AEBSF and 1217 mM^{-1} h^{-1} for GEBSF, which is close to the values obtained by isolated inhibition studies.

Thereafter, we defined three different regions in the batch experiments: I) a delay region during which [Tr] < 1 μM, and inhibition is stronger than autocatalysis, II) a competition region, in which inhibition and autocatalysis compete, and III) a low [Inh] regime, in which most of the inhibitor has already reacted ([Inh] < 0.1 μM). Two batch experiments were simulated, one with AEBSF (84 μM) and one with GEBSF (6.95 μM), that both showed a delay time of 6 h (Fig. 3A). Again, we see that the use of GEBSF results in a steeper rise in trypsin concentration, but now we can also observe that the duration of the competition region is strongly dependent on the inhibition rate constant. In case of GEBSF the competition region is short, as only 2.6 μM of inhibitor is left at the end of the delay region, which is quickly consumed by the autocatalytically formed trypsin. Consequently, at end of the competition region there is still a high concentration of trypsinogen (81 μM), explaining the switch-like behavior. In contrast, the competition region in case of AEBSF is long, as there is still 59 μM of inhibitor present at the start of the competition region, and it ends when trypsinogen is already fully activated. Therefore, the steepness of the trypsin curve is greatly reduced in the latter case, as autocatalysis has to compete with inhibition. Importantly, the concentration of trypsinogen (green lines in Fig. 3A) is similar at the start of the competition region for both AEBSF ([Tg] = 93 μM) and GEBSF ([Tg] = 96 μM), and the differences in steepness of the trypsin curves cannot be attributed to a substrate-depletion effect (*i.e.* that most of the trypsinogen was already converted in the low [Tr] region).

Additional computational analyses showed that the delay time is very sensitive to initial [GEBSF] (orange line in Fig. 3B), while the switch-like behavior – expressed as maximal steepness of the [Tr] curve, or $(d[Tr]/dt)_{max}$ – is retained over a wide range of delay times (orange line in Fig. 3C). In contrast, the delay time increases gradually with increasing [AEBSF] (cyan line in Fig. 3B), and the maximal steepness drops considerably over a small range of delay times (1–4 h, cyan line in Fig. 3C). These results indicate that GEBSF is a better candidate to obtain bistability under flow conditions than AEBSF, because the former has a greater ability to delay the onset of autocatalytic growth whilst still exhibiting switch-like behavior.

2.3. Bistability in flow experiments

Finally, we searched for bistability under flow conditions. We used a 250 μL continuously-stirred tank reactor (CSTR),[16] that was fed by three syringes loaded with either trypsinogen, inhibitor, or a buffer solution (see Experimental Section 4.6 for details). In the syringes, trypsinogen and the inhibitor were kept in acidic solutions to prevent autoactivation and hydrolysis, respectively.

First, however, it is imperative to use a computational model to estimate which inhibitor(s) and conditions are necessary to obtain bistability. The model made in MATLAB contains the same reactions as the COPASI model used to describe the batch experiments, but the former also takes flow into account. Note that flow is hereafter described by space velocity (SV, with units of h^{-1}), which is the ratio of the flow rate (in μL h^{-1}) over the reactor volume (in our case

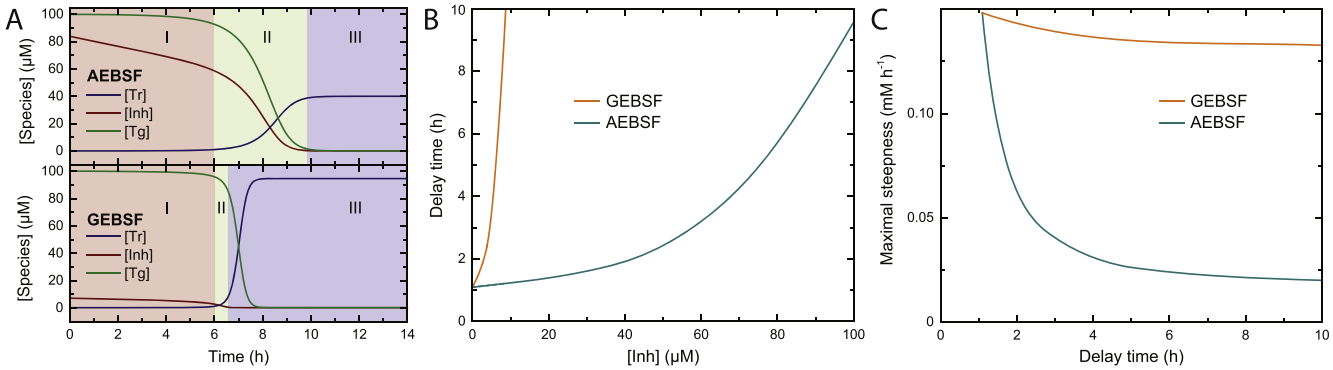

Fig. 3. Modelling batch experiments in COPASI. **A)** Simulation of trypsinogen ($[Tg]_0$ = 100 μM) mixed with either AEBSF (84 μM, top panel) or GEBSF (6.95 μM, bottom panel). Three regions are distinguished: I) Low [Tr] (in red), II) Competition between inhibition and autocatalysis (in green), III) Low [Inh] (in blue. **B)** A plot of the delay time (duration of region I in Figure 3A) *vs* the inhibitor concentration. **C)** A plot of the maximal steepness of the trypsin curve ($(d[Tr]/dt)_{max}$ in mM^{-1} h^{-1}) *vs* the delay time. Abbreviations: Tg = trypsinogen, Tr = trypsin, Inh = inhibitor, AEBSF = 4-(2-aminoethyl)benzenesulfonyl fluoride, GEBSF = 4-(2-guanidinoethyl)benzenesulfonyl fluoride.

250 μL). In the MATLAB model, the space velocity is first increased from 0 (*i.e.* batch conditions) to 4 h^{-1} in small steps. The model waits for 250 simulated hours before changing the space velocity to obtain a final steady state of the system, and uses the final concentrations of compounds in the reactor as the initial conditions at the next space velocity while keeping the inflow concentrations of trypsinogen and inhibitor constant. After reaching a space velocity of 4 h^{-1}, the concentrations in the reactor are set to zero again, and the process is repeated, but now for decreasing space velocity. The system is considered bistable when a difference is observed between the final trypsin concentration obtained at increasing space velocity as compared to the reverse process. Ultimately, the differences in trypsin concentration (Δ[Tr] in μM) are plotted in a phase diagram of initial inhibitor concentration *vs* the space velocity.

Using this model, we did not find bistability in the case of AEBSF, but did observe a large bistable regime for GEBSF (Fig. 4A, $[Tg]_0 = 100$ μM) as expected based on the results of the batch experiments. Finally, we tested the model predictions in flow experiments using the CSTR. We indeed observed bistability and hysteresis in trypsin concentration when the space velocity was first increased, and then decreased again (Fig. 4B). In addition, we observed the same behavior at a constant space velocity, but at changing concentrations of GEBSF (Fig. 4C). The states of high [Tr] are named the thermodynamic branches in Fig. 4B and C, as they resemble the final high [Tr] reached at thermodynamic equilibrium. In contrast, the states of low [Tr] are called flow branch and inhibitor branch in Fig. 4B and C, respectively, since here the antagonists of autocatalysis are dominant. In both flow experiments, we had to wait until at least six reactor volumes of fluid had passed through the reactor for the trypsin concentration to stabilize (the steady-state concentrations of trypsin are plotted in Fig. 4B and C). Additionally, we see that the steady state trypsin concentration is lowered in the thermodynamic branch as the inhibition strength is increased, either by increasing the space velocity or the [GEBSF]. The experimental results are in good agreement with the computational model, although the experimental bistable regime seems to be slightly smaller than the computed one.

3. Conclusion

In this report, we have shown that a combination of synthesis, kinetic studies, batch experiments, and computational modelling resulted in the observation of bistability in a CSTR. Interestingly, we observe that a small change in molecular structure can be crucial for obtaining complex behavior, something we established in previous work as well.[16,17] Our work does not only expand the available toolbox of complex networks, but we also foresee that our bistable system can be implemented in enzyme-responsive, smart materials.[20–23] Furthermore, we expect that strong, natural trypsin inhibitors such as soybean trypsin inhibitor and aprotinin (both are proteins) can also be used to create trypsin-based bistable switches. These alternative inhibitors are interesting for applications where long reaction times may be required, such as in enzyme-responsive materials, as these proteins do not hydrolyze in contrast to the inhibitors used in this study.

4. Experimental section

4.1. Synthesis of 4-(2-N,N′-diboc-guanidinoethyl)benzenesulfonyl fluoride (compound **3**)

N,N′-Di-Boc-thiourea (31.6 mg, 114.7 μmol, 1.2 eq) and 4-(2-aminoethyl)benzenesulfonyl fluoride hydrochloride (AEBSF, 22.9 mg, 95.6 μmol, 1 eq) were first dried under vacuum, and afterwards suspended in dry DCM. Dry *N,N′*-diisopropylethylamine (66 μL, 382 μmol, 4 eq) and fine powdered copper chloride dihydrate (19.6 mg, 114.7 μmol, 1.2 eq) were added in quick succession. The mixture was stirred under nitrogen for one hour, and then poured in 10% (w/v) $KHSO_4$ solution. Next, ethyl acetate was added and the organic phase was separated in a separatory funnel, and subsequently washed with $KHSO_4$ and brine. Then, the mixture was dried over Na_2SO_4, and the solvent was evaporated under reduced pressure. The crude product was purified by silica column chromatography (ethyl acetate/heptane, 1:4, v/v) yielding the desired compound **3** (17.1 mg, 38.2 μmol, 40%).

^{1}H NMR: (400 MHz, CD_3OD) δ 8.14 (d, $J = 8.2$ Hz, 2H), 7.71 (d, $J = 8.3$ Hz, 2H), 3.62 (t, $J = 7.1$ Hz, 2H), 3.14 (t, $J = 7.0$ Hz, 2H), 1.41 (s, 9H), 1.29 (s, 9H); LCQMS-ESI (Da): *m/z* observed 446.38 for $C_{19}H_{29}FN_3O_6S^+$ $[M^+H^+]$; *m/z* calculated for $[M^+H^+]$: 446.18.

4.2. Synthesis of 4-(2-guanidinoethyl)benzenesulfonyl fluoride (GEBSF, compound **4**)

Compound **3** (17.1 mg, 38.2 μmol) was dissolved in 1 mL dioxane, and 1 mL of 4 M HCl in dioxane was added, after which the mixture was stirred overnight at room temperature. Then, the mixture was concentrated under reduced pressure and diethyl ether was added. The formed precipitate was centrifuged, washed two times with diethyl ether, and dried under vacuum yielding the desired compound **4** (GEBSF, 9.7 mg, 34.3 μmol, yield 90%).

^{1}H NMR: (400 MHz, CD_3OD) δ 8.00 (d, $J = 8.2$ Hz, 2H), 7.61 (d,

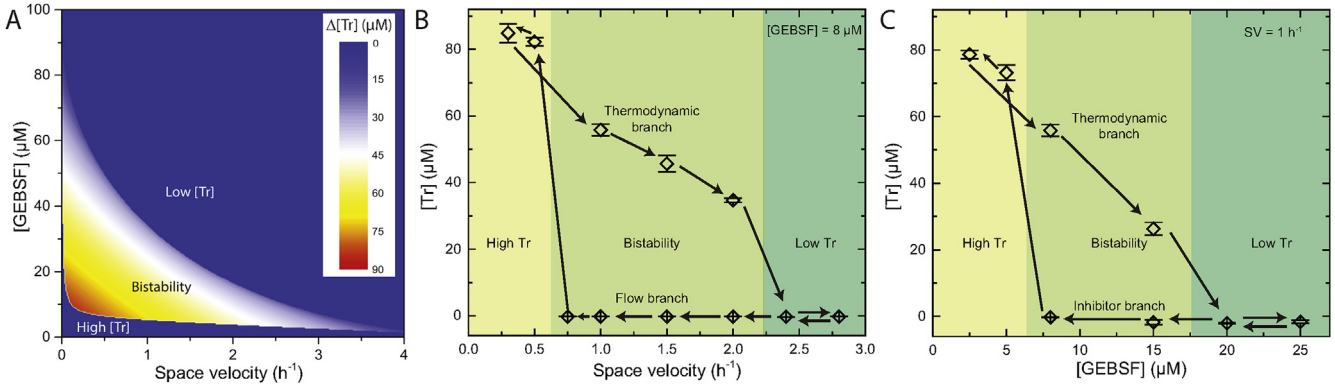

Fig. 4. A) Phase diagram of [GEBSF] *vs* space velocity obtained by simulations in MATLAB. **B)** Bistability in a flow experiment ($[Tg]_0 = 100$ μM, $[GEBSF]_0 = 8$ μM) achieved by changing space velocity once a stable trypsin concentration was reached. **C)** Bistability in a flow experiment ($[Tg]_0 = 100$ μM, SV = 1 h^{-1}) achieved by changing [GEBSF] once a stable trypsin concentration was reached. Error bars in B and C are standard deviations of [Tr] determinations at three different time points, after [Tr] had reached a steady state.

J = 8.1 Hz, 2H), 3.51 (t, J = 7.0 Hz, 2H), 3.02 (t, J = 7.0 Hz, 2H); ^{13}C NMR: (125 MHz, CD_3OD) δ 147.4, 131.3, 131.1, 130.3, 128.4, 41.4, 34.5; LCQMS-ESI (Da): m/z observed 246.28 for $C_9H_{13}FN_3O_2S^+$ [M+H+]; m/z calculated for [M+H+]: 246.07.

4.3. Inhibition of trypsin by GEBSF

Trypsin (29.4 μM) was mixed with GEBSF (40 μM) in 100 mM Tris-HCl, pH 7.7, containing 20 mM $CaCl_2$, and kept at 22 °C. At multiple time points, 20 μL of the reaction mixture was quenched with 180 μL of a 0.1 M $KHSO_4$ solution. 10 μL of the quenched reaction mixture was added to 2.5 mL 50 mM Tris-HCl buffer, pH 7.7, containing 5 μg/mL bis-(Z-Ile-Pro-Arg)-rhodamine 110, a fluorogenic trypsin substrate. Increase in fluorescence intensity (λ_{ex} = 470 nm, λ_{em} = 520 nm) was measured for 20 s, and its slope compared to a calibration curve to calculate the concentration of active trypsin.

4.4. Hydrolysis of GEBSF

GEBSF (0.19 mg, 0.67 μmol, 1.03 mM starting concentration) was dissolved in 650 μL 50 mM Tris-HCl, pD 7.7, in D_2O containing 20 mM $CaCl_2$, and hydrolysis was followed by ^{1}H NMR (400 MHz). The formation of hydrolyzed inhibitor was followed in time by integrating the peaks of the phenyl ring, from which the [GEBSF] over time was calculated.

4.5. Batch experiments

In the batch experiments in Fig. 2, 100 μM of trypsinogen was mixed with varying concentrations of either AEBSF or GEBSF in 100 mM Tris-HCl, pH 7.7, containing 20 mM $CaCl_2$, and kept at 22 °C. The rest of the procedure was identical as described in section 4.3.

4.6. Flow experiments

Details on the fabrication of the CSTR and the experimental setup can be found in our previous work.[16] Three syringes were connected to the reactor, which typically contained: I) trypsinogen (272 μM, 2.40 mg/mL) in 4 mM HCl containing 40 mM $CaCl_2$, II) GEBSF (32 μM in 2 mM HCl), III) 0.5 M Tris-HCl, pH 7.7 buffer. The flow rate for trypsinogen was always half the total flow rate (effective starting concentration [Tg] = 100 μM; note that in the batch used for flow experiments only 74% of trypsinogen was active), and the flow rates of inhibitor and buffer were changed in case different concentrations of inhibitor had to be achieved (in all cases, buffer capacity was at least 50 mM). Droplets from the outlet tubing were collected using a BioRad 2110 fraction collector, in which eppendorf tubes were placed containing 780 μL 0.1 M $KHSO_4$. The quenched solutions were analyzed with the fluorogenic assay described in section 4.3. Droplet volume was determined by measuring the time interval between falling droplets and multiplying this time with the flow rate.

Acknowledgments

The authors thank Britta Helwig for her support during flow experiments. Our work is supported by the European Research Council (ERC; Advanced Grant 246812 Intercom (W.T.S.H.)), the Netherlands Organisation for Scientific Research (NWO, VICI Grant 700.10.44 (W.T.S.H.)), and funding from the Dutch Ministry of Education, Culture and Science (Gravity program 024.001.035).

References

1. Süel GM, Garcia-Ojalvo J, Liberman LM, Elowitz MB. *Nature*. 2006;440:545.
2. Lomakin AJ, Lee K-C, Han SJ, et al. *Nat Cell Biol*. 2015;17:1435.
3. Bagci EZ, Vodovotz Y, Billiar TR, Emmentrout GB, Bahar I. *Biophys J*. 2006;90:1546.
4. Cappell SD, Chung M, Jaimovich A, Spencer SL, Meyer T. *Cell*. 2016;166:167.
5. Santos SDM, Ferrell JE. *Nature*. 2008;454:288.
6. Tyson JJ, Chen K, Novak B. *Nat Rev Mol Cell Biol*. 2001;2:908.
7. Ferrell JE, Xiong W. *Chaos*. 2001;11:227.
8. Kholodenko BN. *Nat Rev Mol Cell Biol*. 2006;7:165.
9. Gardner TS, Cantor CR, Collins JJ. *Nature*. 2000;403:339.
10. Hu G, Pojman JA, Scott SK, Wrobel MM, Taylor AF. *J Phys Chem B*. 2010;114:14059.
11. De Kepper P, Epstein IR, Kustin K. *J Am Chem Soc*. 1981;103:6121.
12. Semenov SN, Kraft LJ, Ainla A, et al. *Nature*. 2016;537:656.
13. Alon U. *Nat Rev Genet*. 2007;4:450.
14. Shah NA, Sarkar CA. *PLOS Comput Biol*. 2011;7:e1002085.
15. Kay J, Kassell B. *J Biol Chem*. 1971;246:6661.
16. Semenov SN, Wong ASY, Van der Made RM, et al. *Nat Chem*. 2015;7:160.
17. Wong ASY, Postma SGJ, Vialshin IN, Semenov SN, Huck WTS. *J Am Chem Soc*. 2015;137:12415.
18. Lachmann H, Schneider FW. *J Am Chem Soc*. 1983;105:2898.
19. Kelly B, Rozas I. *Tetrahedron Lett*. 2013;54:3982.
20. Semenov SN, Markvoort AJ, De Greef TFA, Huck WTS. *Angew Chem Int Ed*. 2014;53:8066.
21. Heuser T, Weyandt E, Walther A. *Angew Chem Int Ed*. 2015;54:13258.
22. Jee E, Bansagi T, Taylor AF, Pojman JA. *Angew Chem Int Ed*. 2016;55:2127.
23. Postma SGJ, Vialshin IN, Gerritsen CY, Bao M, Huck WTS. *Angew Chem Int Ed*. 2017;56:1794.